Supporting Information: Thermal sensitivity across forest vertical profiles: patterns, mechanisms, and ecological implications

Table of Contents

Authors: Nidhi Vinod, Martijn Slot, Ian R. McGregor, Elsa M. Ordway, Marielle N. Smith, Tyeen C. Taylor, Lawren Sack, Thomas N. Buckley, Kristina J. Anderson-Teixeira

Article acceptance date: 31 July 2022.

Notes S1: Biophysical drivers of T_{leaf}

Fundamentally, T_{leaf} is determined by the energy balance and can be estimated based on biophysical principles: $T_{leaf} - T_{air}$ depends on energy input from net radiation (R_n, including shortwave and longwave) minus heat lost to the environment (Fig. 3, Campbell & Norman, 1998; Muir, 2019). High R_n loads can elevate T_{leaf} above T_{air} (Fig. 3a). Sensible heat flux between leaf and air is regulated by leaf boundary layer conductance, which is greater in smaller leaves (Fig. 3d) and under higher wind speeds (Fig. 3b). Latent heat flux (λE) through transpiration cools the leaf, and is determined by stomatal and boundary layer conductances (g_s and g_b) and VPD:g_b increases with wind speed, and g_s generally declines as VPD increases due to stomatal closure (Darwin, 1898; Mott & Parkhurst, 1991). Therefore, $T_{leaf} - T_{air}$ decreases in magnitude with wind speed (Fig. 3b, Daudet *et al.*, 1999), increases with RH (Fig. 3c), increases with leaf size (Fig. 3d), and T_{leaf} decreases absolutely with g_s (Fig. 3e).

Under hot and dry conditions, leaves face a trade-off between T_{leaf} regulation and water conservation (Koch *et al.*, 1994; Fauset *et al.*, 2018). With adequate water, high λE can dissipate excess heat, particularly for smaller leaves (higher g_b) (Leuzinger & Körner, 2007; Dong *et al.*, 2017; Leigh *et al.*, 2017; Song *et al.*, 2020; Konrad *et al.*, 2021). However, when transpiration exceeds water supply, stomata close to conserve water, increasing T_{leaf} (Fig. 3e, Fauset *et al.*, 2018). Therefore, at high solar radiation loads, latent cooling can maintain T_{leaf} closer to T_{air}, but if stomatal opening is limited, solar radiation can drastically elevate T_{leaf} above T_{air}, especially for larger leaves (Fauset *et al.*, 2018; Song *et al.*, 2020; Konrad *et al.*, 2021).

Leaves can be substantially warmer or cooler under certain conditions. They can be warmer than air in full sunlight, especially under slow wind speeds and low T_{air} (Doughty & Goulden, 2008). Leaves are often cooler than the air on clear nights due to radiative coupling with the very cold sky, and under some daytime conditions (cloudy skies, high wind speeds, and high T_{air}, Vogel, 2009; Rey-Sánchez *et al.*, 2016).

Methods S1. Methods for analyzing vertical gradients in the biophysical environment

Study sites

We analyzed vertical gradients in key biophysical variables from the National Ecological Observatory Network's Airborne Observatory Platform (NEON AOP) and meteorology towers at six focal NEON sites (Figs 2, S1, Schimel *et al.*, 2007). The sites are well distributed across the United States and represent key forest types and structures (Table S1).

Estimating forest and light environments from lidar

Data selection

We downloaded classified lidar point clouds as .laz files from the NEON (National Ecological Observatory Network, 2020) data portal. For each site, we analyzed forest structure and light environments using lidar data for the 1 x 1 km plot where the meteorology tower is located. If a large proportion of the plot containing the tower was deforested, we used the closest forested pixel instead. We selected the most recent lidar survey available at each site (all conducted in 2019), which most closely temporally-corresponded to the meteorological time series. All sites were surveyed in growing season months (April-July), except for PUUM (January survey), an evergreen site where total leaf area seasonality is expected to be low.

Lidar data processing

Lidar data were processed according to methods detailed in Stark *et al.* (2012). Outliers on the z plane (height) were removed by applying an interquartile range (IQR) approach. The IQR is calculated as the third quartile (Q3) minus the first quartile (Q1); lidar pulse returns were restricted to > Q1-(1.5xIQR) and < Q3+(1.5xIQR). Next, pulse return counts were quantified, or 'voxelized' within all 2 x 2 x 1 m voxels in a plot.

Digital terrain models (DTMs) were created for each plot using minimum quantile spline regression and interpolation (see Shao et al. 2019) and used to normalize the voxelized lidar data with respect to the ground height. Leaf area density (LAD, $m^2\ m^{-3}$) was estimated by applying the MacArthur-Horn transformation (MacArthur & Horn, 1969) to the voxelized pulse returns. We excluded LAD data at the bottom 5 m of the vertical profile, due to limited pulse penetration within this region furthest away from the sensor (Stark *et al.*, 2012); for calibration purposes, we assumed the bottom 5 m to have a leaf area index (LAI) of 0.25 $m^2 m^{-2}$ (Shao *et al.*, 2019).

We scaled LAD values by a factor of 5.5 so that they matched an independent estimate of LAI. Specifically, published estimates of LAI at SERC (average of 5.78 $m^2\ m^{-2}$) derived from litterfall (Parker *et al.*, 2004), which were then in good agreement with our lidar-derived estimate (5.75 $m^2 m^{-}2$).

Generating leaf area and light transmission profiles.

Site-level LAD profiles were calculated as the mean LAD at each height. Mean light transmission profiles (proportion of incident light) were estimated by applying a vertical light reduction model to LAD estimates (Stark *et al.*, 2012). To estimate the proportion of sun leaves along the vertical profile, we isolated voxels in the upper canopy surface layer (1-2 m from the local canopy surface, likely contain the majority of sun leaves), calculated the mean LAD profile for this surface layer, and divided it by the total mean LAD profile.

Analyzing biophysical gradients from micrometeorological data

Micrometeorological data was downloaded for each site from NEON (neonUtilies R package) at 30 minute intervals for 2015-2020 (National Ecological Observatory Network (NEON), 2022a,b,c,d,e). To focus on the middle of the growing season, the data was constrained to be for the month of July each year. Per site, we calculated the mean maximum and minimum values of each variable by day and by sensor height. In Figure S1 we expanded on Figure 2 by including 22 sites representing five forest structure types.

All data processing, analyses, and graphing were conducted using R (R Core Team, 2021).

Note on interpreting T_{veg}:

Vegetation temperature (T_{veg}) is measured using infrared sensors that integrate across both leaves and woody vegetation. Leaf and branch temperatures often differ substantially; for instance, exposed tropical tree bark can be much warmer than leaves (Pau *et al.*, 2018; Still *et al.*, 2021; Johnston *et al.*, 2022). Thus, vegetation temperature (T_{veg}) does not always equal or approximate T_{leaf}, particularly in settings where leaf area is low relative to woody vegetation (i.e., low-LAI ecosystems and understories).

Methods S2. Methods for leaf energy balance modeling

Energy balance for a typical overstory sun leaf and understory shade leaf were modeled in the R package *tealeaves* (Muir, 2019), parameterized for *Quercus rubra* L. leaves at Harvard Forest, MA, USA (42.5369, -72.17266).

Micrometeorological data from the NEON tower at Harvard Forest (Fig. 2, Supporting Information Methods S1) was used to parameterize biophysical constants, using the mean of maximum PAR, wind speed, and T_{air} for growing season months at vertical positions 60m (overstory) and 10m (understory). Leaf size parameters were selected for *Quercus rubra* sun and shade leaf based on personal observations (by Vinod) and verified as reasonable by Zwieniecki *et al.* (2004).

For the moist scenario, we used mean maximum RH from the NEON tower at Harvard Forest. Stomatal conductance measurements were referred from *Tleaves* typical sun and shade measurements (Muir, 2019) and Cavender-Bares & Bazzaz (2000).

For the drought scenario, we reduced RH to 50% of the mean maximum from the NEON tower at Harvard Forest. For drought PAR values, for the overstory we used the maximum PAR value observed at 60m height on the NEON tower at Harvard Forest, and for the understory we assumed 50% increased PAR relative to the mean daily maximum understory value. We reduced stomatal conductance to a minimum value of 0.01 $\mu mol/m^2/s/Pa$ for both overstory and understory.

In each visual, all biophysical variables are constant except for the independent variable that represents a minimum - maximum range.

Methods S3. Methods for literature review

To summarize vertical gradients in leaf traits and gas exchange (Tables 1-2), we searched the literature for relevant studies and recorded results from all studies meeting our criteria for inclusion.

The studies included in the review were based on a global geographic scope. Ecosystem types included any studies with trees for mostly forests, but savannas were also considered. Herbaceous plant studies and seedling studies were excluded. We targeted studies examining variation in foliar traits and metabolism across independent variables of sun/shade or height (where height is generally also sun/shade). Dependent variables of interest included variables known to influence leaf temperature or metabolism: i.e., anatomical, biochemical, and structural foliar traits; gas exchange, metabolism, and thermal sensitivity variables.

Databases, search terms, and numbers of studies reviewed

We searched for relevant studies using Smithsonian online library, Google Scholar and ISI Web of Science, with the following key terms, resepecitvely:

- (leaf traits OR foliar traits) AND (inter-canopy OR intra-canopy OR canopy height) AND (e.g. chlorophyll OR e.g. LMA OR stomatal conductance)
- (leaf temperature and metabolism OR leaf thermal sensitivity OR leaf thermal tolerance OR leaf traits OR foliar traits) AND (within-canopy OR intra-canopy OR sun shade OR canopy height OR canopy gradient OR canopy profile OR canopy position) AND (temperate forests OR boreal forest OR conifer OR savanna OR tropical)
- (leaf* temperature* and metabolism OR leaf thermal* sensitivity OR leaf thermal tolerance OR leaf* traits OR foliar* traits) AND (within-canopy OR intra-canopy OR sun shade OR canopy* height OR canopy gradient OR canopy profile) AND (temperate forests OR boreal forest OR conifer OR savanna OR tropical).

Through the above process, 202 articles were saved with careful evaluation. To this, additional studies were shared by co-authors.

In total, following careful review, we identified **75** articles as relevant and included their results in Tables 1-2.

Table S1. National Ecological Observatory Network (NEON) sites included in the analysis of vertical gradients of key biophysical characteristics

site code	site name	US state	latitude	longitude	forest type*
BART	Bartlett Experimental Forest Tower	NH	44.06389	-71.28737	Eastern Deciduous Forest, Boreal ecotone
BONA	Bonanza Creek	AK	65.15401	-147.50258	Spruce forest on permafrost
CLBJ	Lyndon B. Johnson National Grassland	TX	33.40123	-97.57000	A mosaic of the Cross Timbers forest (oak-dominated) and grasslands
DEJU	Delta Junction	AK	63.88112	-145.75136	Spruce forest on non-permafrost land
DELA	Dead Lake site	AL	32.54173	-87.80388	Mixed closed-canopy deciduous hardwood forest including cypress, red oak, black gum, shagbark hickory, oaks and green ash
GRSM	Great Smoky Mountains National Park, Twin Creeks	TN	35.68896	-83.50195	Hardwood deciduous forest dominated by oaks and maples
GUAN	Guanica Forest	PR	17.96955	-66.86870	Subtropical dry seasonal forest, dense closed canopy
HARV	Harvard Forest Tower	MA	42.53690	-72.17266	Eastern Deciduous forest
JERC	Jones Ecological Research Center	GA	31.19484	-84.46861	Mixed longleaf pine/hardwood forest
LENO	Lenoir Landing	AL	31.85388	-88.16122	Oak-dominant closed-canopy hardwood forest
MLBS	Mountain Lake Biological Station	VA	37.37828	-80.52484	Eastern Deciduous Forest dominated by Oak
ORNL	Oak Ridge	TN	35.96412	-84.28260	Eastern Uplands Deciduous forest
OSBS	Ordway-Swisher Biological Station	FL	29.68928	-81.99343	Open Longleaf-pine forest
PUUM	Pu‘u Maka‘ala Natural Area Reserve	HI	19.55309	-155.31731	Metrosideros polymorpha-dominated tropical montane forest
SCBI	Smithsonian Conservation Biology Institute	VA	38.89292	-78.13949	Tulip popular and oak dominated closed forest
SERC	Smithsonian Environmental Research Center	MD	38.89013	-76.56001	Hardwood deciduous forest dominant by tulip popular, oak and ash

site code	site name	US state	latitude	longitude	forest type*
SJER	San Joaquin Experimental Range	CA	37.10878	-119.73228	Oak-dominated woodland savanna
SOAP	Soaproot Saddle	CA	37.03337	-119.26219	Pine-dominated forest
STEI	Steigerwaldt Land Services	WI	45.50894	-89.58637	Aspen dominated regenerating forest
TALL	Talladega National Forest	AL	32.95046	-87.39327	Restored longleaf pine forest
TEAK	Lower Teakettle	CA	37.00583	-119.00602	Mixed coniferous forest dominated by red fir, ponderosa and Jeffery pine, white fir, etc.
TREE	Treehaven	WI	45.49369	-89.58571	Restored northern hardwood forest dominated by maple, hemlock, birch, and aspen
UKFS	The University of Kansas Field Station	KS	39.04043	-95.19215	Mixed hardwood forest dominated by oak, hickory, and elm
UNDE	University of Notre Dame Environmental Research Center	MI	46.23391	-89.53725	Northern hardwood forest dominated by sugar maple
WREF	Wind River Experimental Forest	WA	45.80900	-121.98231	Old-growth forest dominated by Douglas-fir, western hemlock, and western red cedar
YELL	Yellowstone Northern Range	WY	44.95348	-110.53914	Open pine-dominated forest

*Refers to forest type around the tower on which the vertical profile of micrometeorological instruments is mounted, as provided by NEON (Hongyan Luo, personal communication; site descriptions on NEON website).

Figure S1. Vertical gradients in micrometeorological conditions for all forested sites in the National Ecological Observatory Network (NEON)

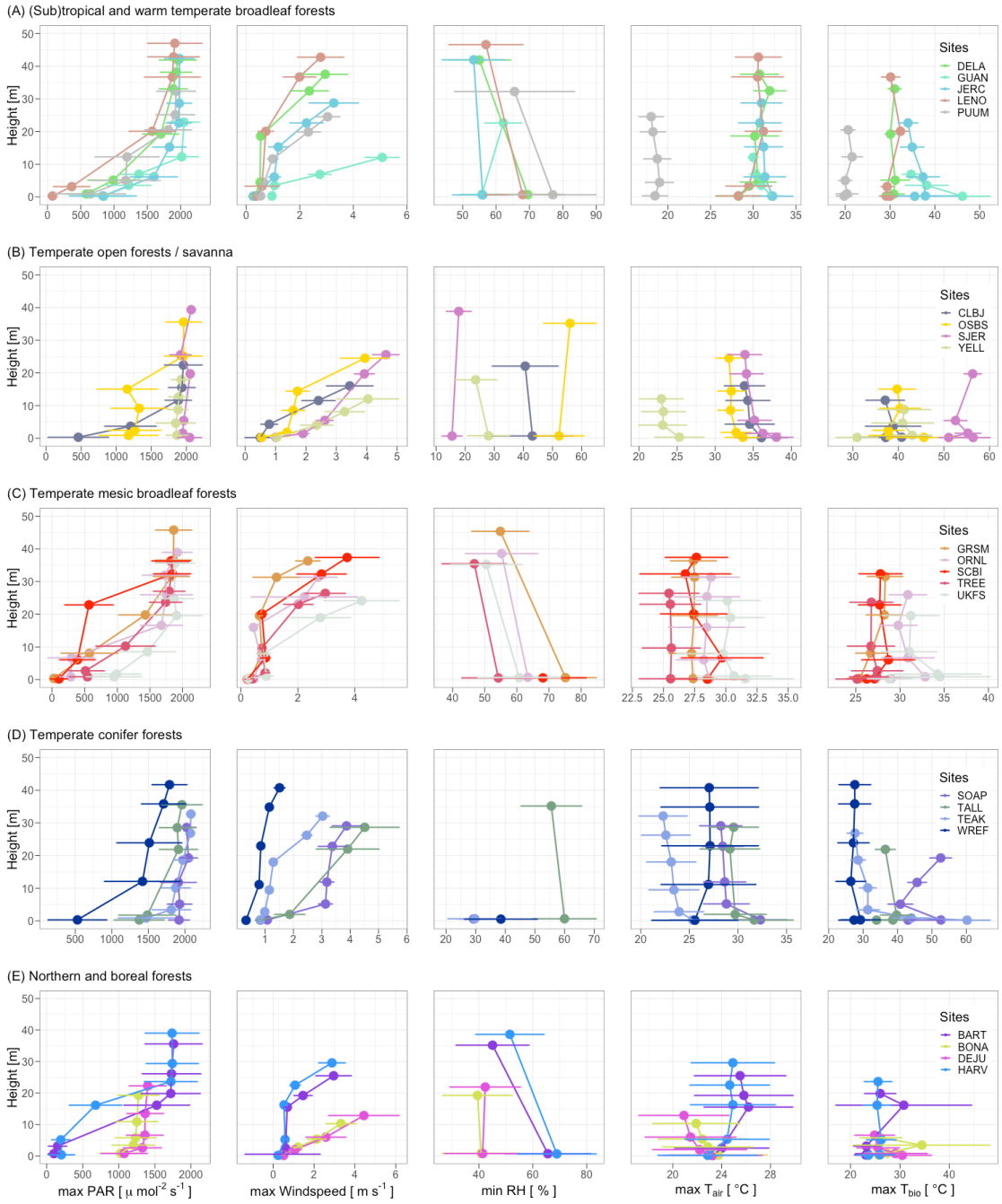

Figure S1. Vertical gradients in micrometeorological conditions for all forested sites in the National Ecological Observatory Network (NEON). *Sites are grouped into five forest types: (sub)tropical and warm temperate broadleaf deciduous forests (A), temperate open forests and savannas (B), temperate mesic broadleaf forests (C), temperate conifer forests (D), and northern and boreal forests (E). Shown are height profiles in July mean ± 1 standard deviation for maximum photosynthetically active radiation (PAR), maximum wind speed,*

minimum humidity, maximum T_{air}, and maximum biological temperature, T_{bio}. Site information is given in Supporting Information Table S1, and analysis details in Supporting Information Methods S1.

References

Campbell G, Norman J. **1998**. *An Introduction to Environmental Biophysics*. New York: Springer.

Cavender-Bares J, Bazzaz FA. **2000**. Changes in drought response strategies with ontogeny in Quercus rubra: Implications for scaling from seedlings to mature trees. *Oecologia* **124**: 8–18.

Darwin F. **1898**. IX. Observations on stomata. *Philosophical Transactions of the Royal Society of London. Series B, Containing Papers of a Biological Character* **190**: 531–621.

Daudet FA, Le Roux X, Sinoquet H, Adam B. **1999**. Wind speed and leaf boundary layer conductance variation within tree crown: Consequences on leaf-to-atmosphere coupling and tree functions. *Agricultural and Forest Meteorology* **97**: 171–185.

Dong N, Prentice IC, Harrison SP, Song QH, Zhang YP. **2017**. Biophysical homoeostasis of leaf temperature: A neglected process for vegetation and land-surface modelling. *Global Ecology and Biogeography* **26**: 998–1007.

Doughty CE, Goulden ML. **2008**. Are tropical forests near a high temperature threshold? *Journal of Geophysical Research: Biogeosciences* **113**: 1–12.

Fauset S, Freitas HC, Galbraith DR, Sullivan MJP, Aidar MPM, Joly CA, Phillips OL, Vieira SA, Gloor MU. **2018**. Differences in leaf thermoregulation and water use strategies between three co-occurring Atlantic forest tree species. *Plant, Cell & Environment* **41**: 1618–1631.

Johnston MR, Andreu A, Verfaillie J, Baldocchi D, Moorcroft PR. **2022**. What lies beneath: Vertical temperature heterogeneity in a Mediterranean woodland savanna. *Remote Sensing of Environment* **274**: 112950.

Koch GW, Amthor JS, Goulden ML. **1994**. Diurnal patterns of leaf photosynthesis, conductance and water potential at the top of a lowland rain forest canopy in Cameroon: Measurements from the Radeau des Cimes. *Tree Physiology* **14**: 347–360.

Konrad W, Katul G, Roth-Nebelsick A. **2021**. Leaf temperature and its dependence on atmospheric CO_2 and leaf size. *Geological Journal* **56**: 866–885.

Leigh A, Sevanto S, Close JD, Nicotra AB. **2017**. The influence of leaf size and shape on leaf thermal dynamics: Does theory hold up under natural conditions? *Plant, Cell & Environment* **40**: 237–248.

Leuzinger S, Körner C. **2007**. Tree species diversity affects canopy leaf temperatures in a mature temperate forest. *Agricultural and Forest Meteorology* **146**: 29–37.

MacArthur RH, Horn HS. **1969**. Foliage Profile by Vertical Measurements. *Ecology* **50**: 802–804.

Mott KA, Parkhurst DF. **1991**. Stomatal responses to humidity in air and helox. *Plant, Cell & Environment* **14**: 509–515.

Muir CD. **2019**. Tealeaves: An R package for modelling leaf temperature using energy budgets. *AoB PLANTS* **11**: 1–8.

National Ecological Observatory Network (NEON). **2022b**. Single aspirated air temperature (DP1.00002.001). https://data.neonscience.org/data-products/DP1.00002.001 (accessed September 1, 2022).

National Ecological Observatory Network (NEON). **2022a**. 2D wind speed and direction (DP1.00001.001). https://data.neonscience.org/data-products/DP1.00001.001 (accessed September 1, 2022).

National Ecological Observatory Network (NEON). **2022c**. IR biological temperature (DP1.00005.001). https://data.neonscience.org/data-products/DP1.00005.001 (accessed September 1, 2022).

National Ecological Observatory Network (NEON). **2022d**. Photosynthetically active radiation (PAR) (DP1.00024.001). https://data.neonscience.org/data-products/DP1.00024.001 (accessed September 1, 2022).

National Ecological Observatory Network (NEON). **2022e**. Relative humidity (DP1.00098.001). https://data.neonscience.org/data-products/DP1.00098.001 (accessed September 1, 2022).

Parker GG, Harding DJ, Berger ML. **2004**. A portable LIDAR system for rapid determination of forest canopy structure. *Journal of Applied Ecology* **41**: 755–767.

Pau S, Detto M, Kim Y, Still CJ. **2018**. Tropical forest temperature thresholds for gross primary productivity. *Ecosphere* **9**: e02311.

R Core Team (2021). R: A language and environment for statistical computing. R Foundation for Statistical Computing, Vienna, Austria.

Rey-Sánchez A, Slot M, Posada J, Kitajima K. **2016**. Spatial and seasonal variation in leaf temperature within the canopy of a tropical forest. *Climate Research* **71**: 75–89.

Schimel D, Hargrove W, Hoffman F, MacMahon J. **2007**. NEON: A hierarchically designed national ecological network. *Frontiers in Ecology and the Environment* **5**: 59–59.

Shao G, Stark SC, de Almeida DRA, Smith MN. **2019**. Towards high throughput assessment of canopy dynamics: The estimation of leaf area structure in Amazonian forests with multitemporal multi-sensor airborne lidar. *Remote Sensing of Environment* **221**: 1–13.

Song Q, Sun C, Deng Y, Bai H, Zhang Y, Yu H, Zhang J, Sha L, Zhou W, Liu Y. **2020**. Tree Surface Temperature in a Primary Tropical Rain Forest. *Atmosphere* **11**: 798.

Stark SC, Leitold V, Wu JL, Hunter MO, de Castilho CV, Costa FRC, McMahon SM, Parker GG, Shimabukuro MT, Lefsky MA, *et al.* 2012. Amazon forest carbon dynamics predicted by profiles of canopy leaf area and light environment. *Ecology Letters* **15**: 1406–1414.

Still CJ, Rastogi B, Page GFM, Griffith DM, Sibley A, Schulze M, Hawkins L, Pau S, Detto M, Helliker BR. **2021**. Imaging canopy temperature: Shedding (thermal) light on ecosystem processes. *New Phytologist* **230**: 1746–1753.

Vogel S. **2009**. Leaves in the lowest and highest winds: Temperature, force and shape. *New Phytologist* **183**: 13–26.

Zwieniecki MA, Boyce CK, Holbrook NM. **2004**. Hydraulic limitations imposed by crown placement determine final size and shape of Quercus rubra L. leaves. *Plant, Cell & Environment* **27**: 357–365.